CRN2 enhances the invasiveness of glioblastoma cells

Anja Ziemann, Simon Hess, Ridhirama Bhuwania, Stefan Linder, Peter Kloppenburg, Angelika A. Noegel, and Christoph S. Clemen

Center for Biochemistry, Institute of Biochemistry I, Medical Faculty (A.Z., A.A.N., C.S.C.), Institute of Zoology (S.H., P.K.), Center for Molecular Medicine Cologne (S.H., P.K., A.A.N.), and Cologne Excellence Cluster on Cellular Stress Responses in Aging-Associated Diseases, University of Cologne, Cologne (S.H., P.K., A.A.N.); and Institute of Medical Microbiology, Virology and Hygiene, University Medical Center Hamburg-Eppendorf, Hamburg, Germany (R.B., S.L.)

Background. Movement of tumor cells involves dynamic remodeling of the actin cytoskeleton, which is regulated by actin binding proteins, such as CRN2 (synonyms: coronin 1C, coronin 3). In vitro, CRN2 participates in secretion, matrix degradation, protrusion formation, and cell migration. Furthermore, expression of CRN2 correlates with the malignant phenotype of human diffuse gliomas. CRN2's effects on actin polymerization and F-actin bundling are abolished by protein kinase 2 (CK2) dependent phosphorylation at serine 463.
Methods. We generated human U373 glioblastoma cell lines with knock-down of CRN2 or over-expression of CRN2 variants and studied their behavior in vitro and ex vivo in organotypic brain slice cultures.
Results. CRN2 over-expression and expression of the S463A phospho-resistant CRN2 variant increase proliferation, matrix degradation, and invasion but decrease adhesion and formation of invadopodia-like extensions in vitro. Knock-down of CRN2 and expression of S463D phospho-mimetic CRN2 generally have opposite effects. Analysis of invadopodia-like cell extensions shows a diffuse relocalization of F-actin in CRN2 knockdown cells, whereas expression of S463A and S463D mutant CRN2 causes enrichments of F-actin structures at the center and rime zone, respectively. Fluorescence recovery after photobleaching studies of CRN2 and F-actin in lamellipodia show that both CRN2 variants decrease the turnover of actin filaments. Glioblastoma cells over-expressing wild-type or S463A CRN2, which were transplanted onto brain slices, characteristically developed into tumors with an invasive phenotype.
Conclusions. Overall, our data indicate that CRN2 participates in cancer progression via modulation of the actin cytoskeleton.

Keywords: actin cytoskeleton, brain slice culture, cancer, coronin 1C, coronin 3, invasion.

Corresponding Authors: Christoph S. Clemen, MD, Institute of Biochemistry I, Medical Faculty, University of Cologne, Joseph-Stelzmann-Str. 52, 50931 Cologne, Germany (christoph.clemen@uni-koeln.de); Angelika A. Noegel, PhD, Institute of Biochemistry I, Medical Faculty, University of Cologne, Joseph-Stelzmann-Str. 52, 50931 Cologne, Germany (noegel@uni-koeln.de).

Coronin proteins belong to the super family of eukaryotic-specific WD40-repeat domain proteins.[1] Phylogenetic analyses of the coronin family of proteins defined 17 coronin subfamilies, including 7 paralogs in mammals.[2-4] CRN2 is a 474 amino acid short coronin[5] harboring 7 WD40-repeats, which adopt the fold of a 7-bladed β-propeller.[6,7] It has an apparent molecular mass of 57 kDa (reference sequences: NM_014325.2, NP_055140.1). Coronin proteins function in cellular actin dynamics and play important roles in numerous cellular processes, for example, in secretion, matrix degradation, protrusion formation, cell migration, and invasion.[8] CRN2 homo-trimerizes via its C-terminal coiled coil domain and binds to and bundles actin filaments via 3 actin binding sites.[9-12] CRN2's F-actin bundling activity and inhibitory effect on actin polymerization are abolished by CK2-dependent phosphorylation of CRN2 at serine 463, as shown by in vitro and in vivo kinase assays and the use of S463D phospho-mimetic and S463A phospho-resistant CRN2 variants.[12] In addition, CRN2 regulates the actin cytoskeleton via interaction with small G-proteins. An interaction of CRN2 with GDP-Rab27a increased its F-actin

bundling activity and endocytosis of the insulin secretory membrane in pancreatic beta cells.[4,13]

With respect to human cancer, the number of CRN2 positive tumor cells is correlated with the malignant phenotype of human diffuse gliomas. Gliomas of high grade, such as anaplastic astrocytomas, anaplastic oligodendrogliomas, anaplastic oligoastrocytomas, and glioblastomas, show high numbers of CRN2-positive tumor cells, whereas low-grade gliomas, such as diffuse astrocytomas, oligodendrogliomas, and oligoastrocytomas, show low numbers of CRN2-positive tumor cells.[14] Furthermore, CRN2 expression is up-regulated in melanoma cells.[15] In another study, the expression level of CRN2 correlated with the clinical progression of hepatocellular carcinoma.[16] Finally, the CRN2 gene was amplified in one-fourth and the CRN2 expression was elevated in three-fourths of the specimens of primary effusion lymphoma.[17] In the present work, we show that increased expression of CRN2 or presence of the S463A phospho-resistant mutant promote glioblastoma cell invasion in vitro and tumor growth ex vivo, whereas knock-down of CRN2 or expression of the S463D phospho-mimetic variant causes opposite effects.

Materials and methods

Generation of Lentivirally Transduced Human U373 Glioblastoma Cells

Six different U373 human glioblastoma cell lines (wild-type: ECACC 89081403) were generated. First, U373 cells with a stable knock-down (oligo cgtccactacctcaacacatt[14]) of CRN2 were generated according to the method described in Thal et al.[14] Second, for U373 cells expressing GFP alone, a CMV-GFP cassette (blunted AseI/sticky EcoRI fragment derived from pEGFP-C1 [Clontech 6084-1]) was inserted between the U6 promoter and the central polypurine tract of the empty pLKO.1-puro (blunted AgeI/sticky EcoRI opened backbone [OpenBiosystems RHS4078]), resulting in pLKO.1-CMV-EGFP-puro. Third, for U373 cells expressing GFP-CRN2, first, a multiple cloning site was inserted into the EcoRI site of pLKO.1-CMV-EGFP-puro, resulting in pLKO.1-CMV-EGFP-MCS-puro, and second, the CRN2-cassette previously cloned into pEGFP-C1[10] was transferred as PstI/SmaI fragment into the PstI/EcoRV opened multiple cloning site. Finally, a primer duplex was inserted into the PstI site of the construct to extend the linker between GFP and CRN2 and to correct the reading frame resulting in pLKO.1-CMV-EGFP-CRN2-puro. Fourth, for U373 cells either expressing GFP alone or wild-type, phospho-resistant S463A, or phospho-mimetic S463D variants of GFP-CRN2 fusion proteins in the background of the knockdown of the endogenous CRN2, first, the puromycin selection cassette of pLKO.1-CMV-EGFP-MCS-puro was removed by BamHI/NsiI digestion and replaced by a neomycin cassette retrieved as PCR product from pEGFP-C1 with adjacent BamHI and NsiI restriction sites, resulting in pLKO.1-NEO-CMV-EGFP-MCS.

Second, the CRN2-cassettes, which are resistant to the above shRNA oligo and code for either serine, aspartic acid, or alanine at position 463, were retrieved as PstI/SmaI fragments from pEGFP-CRN2res-WT, pEGFP-CRN2res-S463A, and pEGFP-CRN2res-S463D,[12] respectively, and transferred to the PstI/EcoRV opened pLKO.1-NEO-CMV-EGFP-MCS. Finally, after insertion of the primer duplex as in the third, constructs pLKO.1-NEO-CMV-EGFP-CRN2res-WT, pLKO.1-NEO-CMV-EGFP-CRN2res-S463A, and pLKO.1-NEO-CMV-EGFP-CRN2res-S463D were obtained. Differing from the transduction protocol described in Thal et al,[14] the U373 target cells were transduced at 24 h and 72 h, with viral supernatants carrying the puromycin resistance, and at 48 h and 96 h, with viral supernatants carrying the neomycin resistance obtained from transfection of the 293TN pseudoviral particle producer cells (BioCat/SBI: LV900A-1). Further selection of the U373 cells was done with 0.75 μg/mL puromycin and/or 400 μg/mL neomycin starting 8 h after the last infection cycle. Cells were grown in Dulbecco's modified Eagle's Medium (4.5 g/L glucose, PAA) supplemented with 10% fetal calf serum (Biochrom), 1 mM sodium pyruvate, 0.1 mM non-essential amino acids, 2 mM L-glutamine (Sigma), 100 U/mL penicillin G, and 100 μg/mL streptomycin (Invitrogen) at 5% CO_2 and 37°C.

Organotypic Brain Slice Cultures

After anesthesia (Forene, Abbott), 9–12-day-old C57BL/6N mice were decapitated, brains were dissected, the frontal poles of the hemispheres and the cerebella removed, and coronal slices of 350 μm prepared with a vibratome (Leica VT100S) in cold (4°C) carbogenated (95% O_2, 5% CO_2) glycerol-based modified artificial cerebrospinal fluid (GaCSF, ~310 mosm/L[18]; 10 mM Hepes-NaOH, 21 mM $NaHCO_3$, 1.2 mM NaH_2PO_4, 2.5 mM KCl, 2 mM $MgCl_2$, 2 mM $CaCl_2$, 5 mM glucose, 250 mM glycerol, pH 7.2). Brain slices were immediately transferred into carbogenated preparation medium (16 mg/mL MEM powder, 10 mM Trismabase, 100 mg/mL D-glucose, 4 mM L-glutamine, 25% horse serum, pH 7.4). Brain slices were grown on tissue culture inserts (0.4 μm pore size 6-well culture inserts or 8 μm pore size 24-well culture inserts FluoroBlok inserts; Falcon) at 37°C and 5% CO_2 containing prewarmed cultivation medium (25% HBSS, 8 mg/mL MEM powder, 5 mM Trisma-base, 0.04% Na_2CO_3, 120 mg/mL D-glucose, 4 mM L-glutamine, 0.8 mg/mL vitamin C, 4 μg/mL insulin, 100 U/mL penicillin, 0.1 mg/mL streptomycin, 25% horse serum, pH 7.4).

After 3 days of culture, ~5000 U373 human glioblastoma cells (0.05 μL; 100 000 cells/μL) were transplanted (0.5 μL Hamilton 7000.5KH syringe) on the entorhinal cortex.[19] This area of the brain and the hippocampal formation still develop postnatal, are still networked in the slice format, and can be kept in culture for many days.[20] Within 2 days, the transplanted U373 cells developed into tumors. Slices were fixed in a 4% paraformaldehyde solution for 30 min and washed 3 times

with PBS 10 min each. The semiporous membranes with the adhered fixed slices were cut from the culture inserts and placed upsidedown in PBS in imaging dishes (Ibidi 81156) for confocal microscopy. Images were recorded at $100 \times$ magnification (objective HCX PL APO CS 10.0×0.40 DRY UV) and 3 μm z-axis step size for whole tumor overviews.

Tumor morphology was evaluated after 3D image reconstruction to differentiate between a spherical and an irregular (i.e., not ball-like, but with cells spreading in multiple directions) morphology. The size of the tumor infiltration area was calculated from the pixel count of the tumor area in the maximum projection of the z-stacks. The tumor infiltration depth was determined as the distance between the uppermost and lowermost z-level that contained tumor cells.

In Vitro Cell Assays

Cell adhesion to a confluent monolayer of primary human aortic endothelial cells (Genlantis, PH30405AK) was measured using the CytoSelect Tumor-Endothelium Adhesion Assay (Cell Biolabs, CBA-215) according to the manufacturer's protocol. For this assay, the U373 glioblastoma cells were labeled with a fluorescent dye (CytoTracker), seeded on the nonlabeled endothelial cells, and allowed to adhere for 1 h. After washing steps and cell lysis, the fluorescence intensity was measured to quantitate the amount of adherent U373 cells. Invasion and passage of U373 cells through a collagen I–coated semiporous membrane was analyzed using the CytoSelect 96-Well Cell Invasion Assay (Cell Biolabs, CBA-112-COL) according to the manufacturer's protocol. Here, the U373 cells were seeded on the collagen I–coated membrane and allowed to invade the collagen I matrix and to pass through the membrane pores. After 18 h, cells that clinged below the membrane were lysed, DNA was fluorescently labeled (CyQuantGR dye), and the amount of cells was determined by fluorescence intensity measurement. To determine proliferation rates, 7×10^4 U373 cells were seeded in duplicate into 60 mm diameter culture dishes; they were trypsinized and counted again after 24 h and 48 h. Invadopodia formation in conjunction with collagen I matrix degradation was analyzed according to Thal et al.[14] In brief, the U373 cells were seeded at low density on cover slips coated with Alexa Fluor-568–labeled gelatin. Cells were grown for 24 h, fixed, and stained with Alexa Fluor-647–labeled Phalloidin. Invadopodia are visible as F-actin spots that colocalize with the degradation of the fluorescently labeled gelatin matrix. Shape of invadopodia-like structures and organization of their internal actin cytoskeleton were monitored on the basis of the method described by Schoumacher et al[21] with the following modifications. U373 cells were seeded on 3 μm pore size membrane inserts in a 24-well format (Falcon). The membranes were coated with collagen I without sealing the pores. Cells were fixed in 4% paraformaldehyde, F-actin was stained by TRITC-phalloidin, and the membranes were further processed as described

above. Images were recorded at $1000 \times$ magnification (objective HCX PL APO CS 100.0×1.40 OIL) and 0.5 μm z-axis step size.

Fluorescence Recovery after Photobleaching Experiments

U373 glioblastoma cell lines expressing the above GFP-CRN2 constructs were transiently transfected (Nucleofector II electroporation device, Amaxa/Lonza) with a plasmid coding for mCherry-actin[22] (provided by Klemens Rottner, University of Bonn, Germany). Fluorescence recovery after photobleaching (FRAP) analyses were performed to determine the dynamics of the GFP-CRN2 proteins in relation to the F-actin network in the front of lamellipodia. Imaging dishes with U373 cells were placed in a stage-top incubator (Leica) for a humidified 5% CO_2 atmosphere (gas mixer "The Brick," Life Imaging Services). For 37°C warm air incubation, the microscope, including stage-top incubator and objectives, was encased (heater "The Cube" and casing "The Box," Life Imaging Services). Settings were as follows: objective HCX PL APO lambda blue 63.0×1.40 OIL UV, 512×512 pixel resolution, bidirectional x-line scanning at 1000 Hz, pinhole 280 μm, photobleaching at fly mode with 100% laser light intensities (405, 458, 476, 488, and 561 nm), image recording at 495 nm-550 nm for GFP and 575 nm-601 nm for mCherry with 2-line average. Three images were acquired before 3 bleaching iterations diminished the fluorescence signals within the region of interest (ROI, 1.5 μm × 3 μm). Recovery of fluorescence was observed for 20 subsequent frames. Raw data (ROI and whole cell intensities) were first background corrected, followed by a correction of photobleaching of the ROI values using the whole cell intensity at each time point, and then normalized to the prebleach intensity. Resulting values were used to calculate the mobile fraction and half-life time of recovery via double-exponential curve fitting (solver add-in of Microsoft Excel). To restrict the analyses to dynamic lamellipodia, cells only with half-life times up to 10 s were used for final statistical evaluation and graphical presentation.

Miscellaneous Methods

Immunoblotting was performed according to Clemen et al[23]. Monoclonal antibodies (mAb) used were directed against CRN2, K6-444 mouse mAb;[10] GFP, K3-184 mouse mAb;[24] α-tubulin, YL1/2 rat mAb;[25] and GAPDH, mouse mAb (Sigma G9295). Cell adhesion and invasion assays were analyzed using an Infinite M1000 plate reader (Tecan, software i-control, version 1.9.17.0). All microscopic images (emission detection in sequential mode) and FRAP raw data were acquired using a TCS SP5 confocal laser scanning microscope (Leica, software LAS AF, version 2.6.0.7266). Data analyses and statistical evaluations were performed using Excel 2010 (Microsoft); the number of independent experiments, mean values, standard errors, and P values (Student's t test) are indicated. Images were processed and figures mounted using CorelDraw Graphics Suite X4.

Results

Knock-Down of CRN2 and Expression of the S463D Phospho-Mimetic CRN2 Variant Inhibit Proliferation and Invasion but Stimulate Adhesion of U373 Glioblastoma Cells In Vitro

We used U373 human glioblastoma cells with a stable and effective shRNA-mediated knock-down of the endogenous CRN2. In these cells, using a second lentiviral transduction approach, we stably expressed GFP-CRN2 fusion proteins that either corresponded to wild-type CRN2 (CRN2-shRNA/GFP-CRN2-WT), a phospho-resistant protein (CRN2-shRNA/GFP-CRN2-S463A), or a phospho-mimetic protein (CRN2-shRNA/GFP-CRN2-S463D). For control, GFP alone was also expressed in the knockdown cells (CRN2-shRNA/GFP). Furthermore, we included U373 cells in our assays that over-expressed GFP-CRN2 or GFP in the presence of the endogenous CRN2 (Fig. 1). This set of cells allows analysis of CRN2-specific and CRN2 phosphorylation–specific cellular effects.

To study the role of CRN2 in tumor-related cellular processes, we performed several in vitro assays. Cell proliferation assays showed the lowest mean fold change in the number of cells for CRN2-shRNA/GFP cells ($\times 1.9$), which were used as reference. Presence of the endogenous CRN2 in cells expressing only GFP (GFP cells) slightly increased the proliferation rate by 7%, which
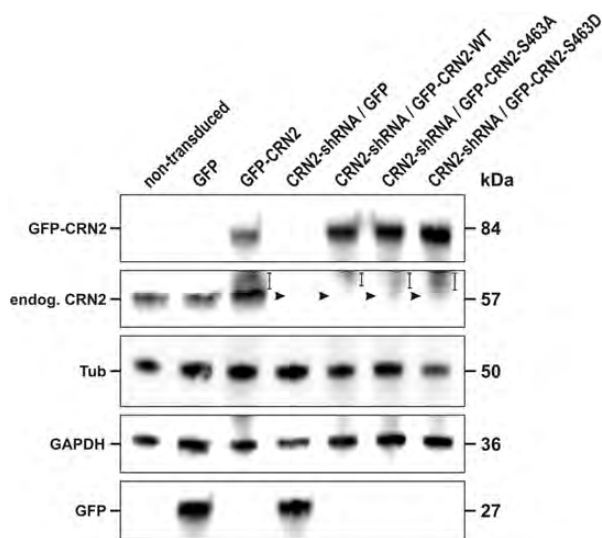

Fig. 1. Generation of U373 cell lines with knock-down of CRN2 and/or over-expression of CRN2 variants. Immunoblotting demonstrates the presence of endogenous CRN2 in nontransduced and GFP-expressing control cells. Cells over-expressing GFP-CRN2, in addition to endogenous CRN2 show signals at 57 and 84 kDa. In CRN2 knock-down cell lines (CRN2-shRNA) expressing GFP-CRN2-WT, GFP-CRN2-S463A, or GFP-CRN2-S463D, an 84 kDa fusion protein is detected; endogenous CRN2 is missing (arrowheads). CRN2 and GFP-tagged CRN2 were detected with mAb K6-444, GFP with mAb K3-184. Distance labels, unspecific background. Presence of protein in all samples was confirmed by α-tubulin and GAPDH antibodies.

increased significantly further in case of GFP-CRN2, CRN2-shRNA/GFP-CRN2-WT, and CRN2-shRNA/GFP-CRN2-S463A cells by ∼21%. No difference was observed between CRN2-shRNA/GFP and CRN2-shRNA/GFP-CRN2-S463D. However, CRN2-shRNA/GFP-CRN2-S463D cells showed a significant decrease by 18%, compared with both CRN2-shRNA/GFP-CRN2-WT and CRN2-shRNA/GFP-CRN2-S463A cells (Fig. 2A). An analysis of the U373 cell adhesion to a monolayer of primary human aortic endothelial cells demonstrated highest levels in CRN2-shRNA/GFP cells, as determined by relative fluorescence intensity measurements of adherent cells (56 000 RFU). Although no obvious change was observed for CRN2-shRNA/GFP-CRN2-WT cells, significant reductions by up to 37% of the adhesion capacity of CRN2-shRNA/GFP cells were observed for CRN2-shRNA/GFP-CRN2-S463D, GFP-CRN2, CRN2-shRNA/GFP-CRN2-S463A, and GFP cells. In addition, CRN2-shRNA/GFP-CRN2-S463A and CRN2-shRNA/GFP-CRN2-S463D cells showed reductions of adhesion by 34% and 10%, respectively, compared with CRN2-shRNA/GFP-CRN2-WT cells (Fig. 2B). For quantitation of matrix degradation, which was determined by the presence of invadopodia (F-actin core) and absence of the matrix signal (Alexa Fluor-568-gelatin), the cell lines were seeded on gelatin-coated cover slips. The CRN2-shRNA/GFP reference cells exhibited the lowest matrix degradation activity (0.37% degradation area per cell area); GFP and CRN2-shRNA/GFP-CRN2-WT cells showed a certain increase. Significantly increasing matrix degradation rates were observed for CRN2-shRNA/GFP-CRN2-S463D, CRN2-shRNA/GFP-CRN2-S463A, and GFP-CRN2 cells, with an increase of up to 346%. CRN2-shRNA/GFP-CRN2-S463A cells showed slightly higher activities, compared with CRN2-shRNA/GFP-CRN2-WT and CRN2-shRNA/GFP-CRN2-S463D cells (Fig. 2C). Invasion capacity of the U373 glioblastoma lines was further analyzed using a Boyden chamber with an 8 μm pore size membrane coated with collagen I in a 96-well format. The ability to degrade the collagen matrix barrier and to pass through the membrane pores was lowest in CRN2-shRNA/GFP (727 RFU) and CRN2-shRNA/GFP-CRN2-S463D cells (606 RFU). While there was a slight increase of invasion of CRN2-shRNA/GFP-CRN2-WT cells, significant changes were observed in case of GFP cells with a moderate and of CRN2-shRNA/GFP-CRN2-S463A and GFP-CRN2 cells with a marked increase by up to 98%, compared with CRN2-shRNA/GFP cells. Compared with CRN2-shRNA/GFP-CRN2-WT cells, CRN2-shRNA/GFP-CRN2-S463A cells showed an increase by 54%, whereas CRN2-shRNA/GFP-CRN2-S463D cells displayed a decrease by 27% (Fig. 2D). Overall, the data indicate that increased U373 glioblastoma cell proliferation, matrix degradation, invasion rates and a decreased cell adhesion are associated with an elevated level of CRN2 expression. However, this is not valid for the S463D mutant CRN2, which, except for the matrix degradation, is comparable to the CRN2 knockdown cells. From this, we hypothesized
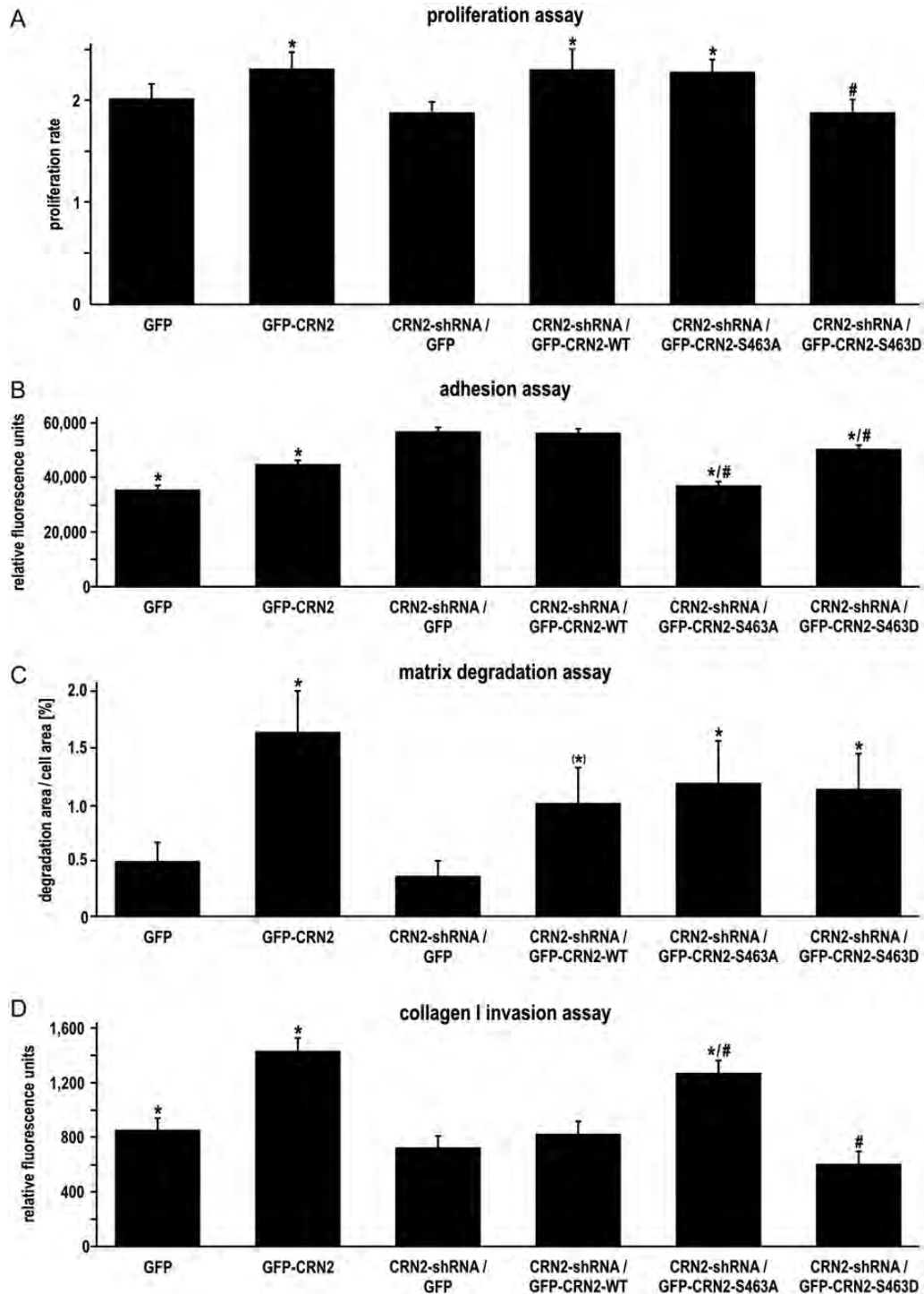
Fig. 2. Involvement of CRN2 in cell proliferation, adhesion, matrix degradation, and invasion. (A) To determine the proliferation rate, 7×10^4 cells per cell line were seeded into 60 mm plates at day 0 and counted at day 1 and day 2. For each cell line, the mean proliferation rate between day 1 and day 2 and the standard errors were calculated from 12 measurements derived from 4 independent experiments. (B) Adhesion of the U373 tumor cell lines (1×10^5 cells/well of a 96-well plate) to a monolayer of primary human aortic endothelial cells was quantitated using a fluorescence-based protocol. Mean adhesion values and standard errors were calculated from measurements of 16 wells. (C) Matrix degradation in conjunction with the formation of invadopodia was determined using fluorescently labeled gelatin. Invadopodia at the ventral surface of the cells are defined by presence of an F-actin core, matrix degradation by the loss of the TRITC-gelatin signal. The total area of matrix degradation per cell was normalized to the cell area. Mean values per cell line and standard errors were calculated from 30 different cells derived from 3 independent experiments. (D) 0.2×10^5 U373 cells per well were seeded on the upper surface of a collagen I−coated semi-porous membrane in a 96-well format. The number of cells that had invaded the collagen matrix and migrated to the lower surface of the membrane (principle of a Boyden chamber) was quantitated by a fluorescence measurement. Mean values and standard errors were calculated from 16 measurements per cell line. *Statistically significant changes, compared with CRN2-shRNA/GFP cells. #Statistically significant changes, compared with CRN2-shRNA/GFP-CRN2-WT cells. See Table 2 for P values.

that glioblastoma cells over-expressing wild-type or S463A CRN2 exhibit an increased tumorigenicity.

Expression Level and Phosphorylation State of CRN2 Are Essential Parameters of Tumor Invasiveness Ex Vivo

To address the biological role of CRN2 in tumor formation, we used organotypic brain slice cultures. Within 2 days, the U373 cells, which were transplanted onto the entorhinal cortex, developed into tumors, and this process was monitored by confocal laser scanning microscopy. 3D image reconstruction showed that tumors formed by CRN2-shRNA/GFP cells rarely (22% of cases) developed into irregular tumors; instead, they mostly had a ball-like shape. In contrast, cells expressing endogenous CRN2 (GFP cells) mostly (60%) and GFP-CRN2 over-expressing cells always (100%) formed tumors that had an irregular and widespread morphology. The majority of tumors grown from CRN2-shRNA/GFP-CRN2-WT and CRN2-shRNA/GFP-CRN2-S463A cells also had a highly irregular and widespread shape (85% and 81%, respectively), whereas in case of CRN2-shRNA/GFP-CRN2-S463D cells, fewer tumors showed an irregular morphology (77%). The spherical tumors observed for CRN2-shRNA/GFP-CRN2-S463D cells (23% of cases) had similar morphology as the ones grown from CRN2-shRNA/GFP cells, however, with a more infiltrating tumor border (Figs. 3 and 4A).

Tumor invasion area and infiltration depth were determined after 2 days of growth. Tumor areas exceeding $100\,000\ \mu m^2$ ($1 \times 10^{-7}\ m^2$) were categorized as large,

and others were considered to be small. The invasion was lowest in tumors grown from CRN2-shRNA/GFP cells, with only 33% of cases having a large infiltration area. A certain increase was determined for tumors formed by GFP (60% of cases) and GFP-CRN2 cells (67%). Further significant increases were observed for CRN2-shRNA/GFP-CRN2-WT and CRN2-shRNA/GFP-CRN2-S463D cells (both 85%) and for CRN2-shRNA/GFP-CRN2-S463A cells (91%) (Fig. 4B). The infiltration depth was similarly categorized into high ($>100\ \mu m$) and low ($\leq 100\ \mu m$). Compared with CRN2-shRNA/GFP cells, which showed less invasion, with only 22% of cases having a high infiltration depth, CRN2-shRNA/GFP-CRN2-S463D (31% of cases), CRN2-shRNA/GFP-CRN2-WT (46%), GFP (50%), CRN2-shRNA/GFP-CRN2-S463A (55%), and GFP-CRN2 (56%) cells exhibited an increasing number of tumors with high infiltration depth (Fig. 4C). The results from these ex vivo experiments indicate that the malignancy of tumors grown from the transplanted U373 glioblastoma cell lines is associated with an elevated level of CRN2. When comparing the mutant CRN2 versions, GFP-CRN2-S463A and GFP-CRN2-S463D caused a more malignant phenotype than the knock-down of CRN2, with GFP-CRN2-S463A showing the most enhanced malignancy.

F-Actin Patches in Cell Extensions Are Lost after CRN2 Knock-Down and Change their Localization Depending on the Phosphorylation Status of S463

To further explore the observed differences in U373 glioblastoma cell invasion, cells were seeded on 3 μm pore
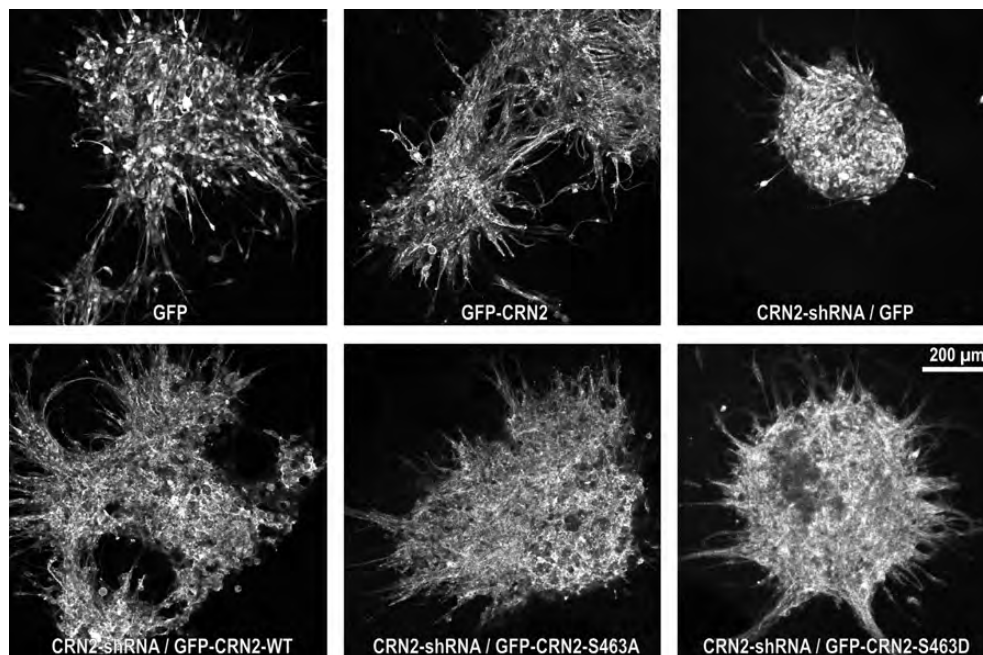
Fig. 3. Increased levels of CRN2 or presence of the S463A phospho-resistant CRN2 variant causes the formation of an irregular tumor morphology; 5000 U373 human glioblastoma cells per cell line were transplanted onto the surface of the entorhinal cortex of mouse brain slice cultures. The transplanted cells developed into tumors, and their growth was monitored by confocal microscopy. Representative images (GFP-fluorescence signal) are shown.
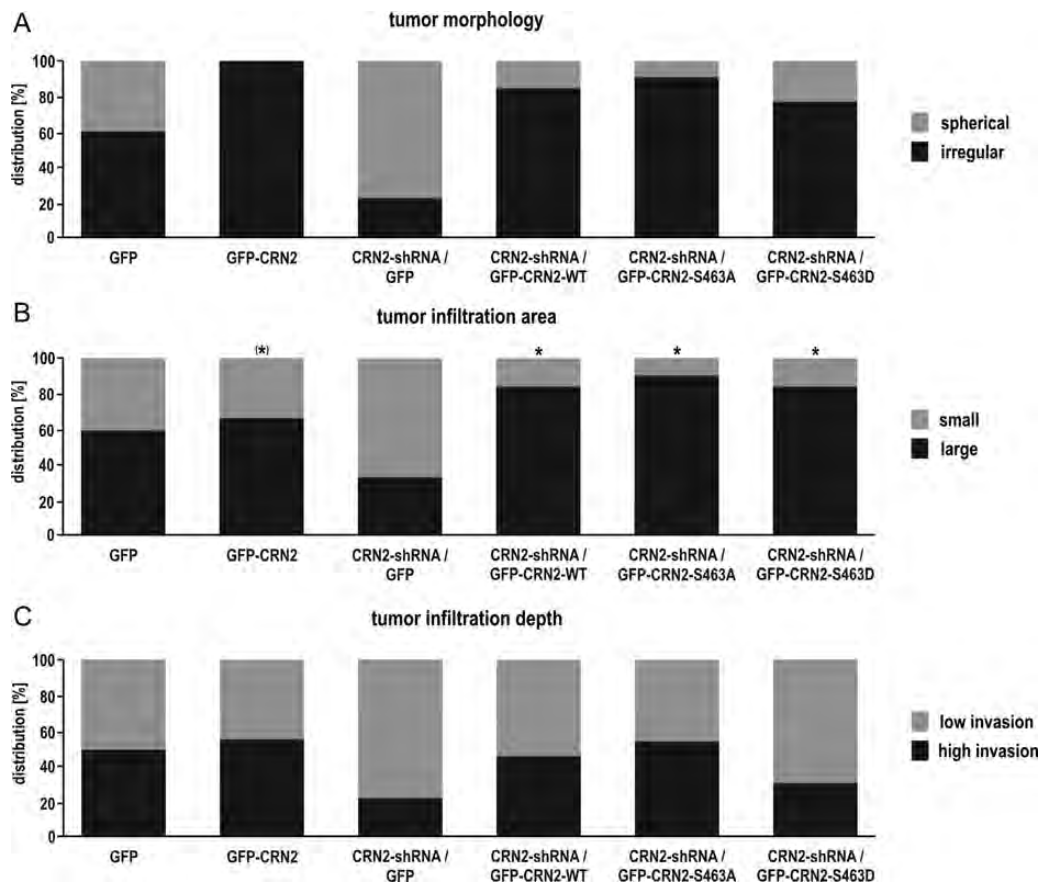
Fig. 4. Increased levels of CRN2 or presence of the S463A phospho-resistant CRN2 variant lead to a more invasive tumor phenotype. Morphology (spherical or irregular [A]), area of infiltration (small, or large $>1 \times 10^{-7}$ m^2 [B]), and infiltration depth (low, or high >100 μm [C]) of the tumors formed by the U373 cells, as seen in Fig. 3, were quantitated, and distributions are shown as stacked columns. A number of 9–13 tumors were analyzed per cell line. *Statistically significant changes, compared with CRN2-shRNA/GFP cells; see Table 2 for *P* values.

size membrane inserts in a 24-well format. Invadopodia-like extensions[26,27] that grew from the ventral cell surface through the pores were analyzed by 3-dimensional confocal laser scanning microscopy (Fig. 5A). Compared with CRN2-shRNA/GFP cells (77% mean number of extensions per number of membrane pores that were covered by a cell), the GFP, GFP-CRN2, and CRN2-shRNA/GFP-CRN2-S463D cells had a decreased number of extensions (values of 63%, 65%, and 63%), whereas no change and an increased value were detected for CRN2-shRNA/GFP-CRN2-WT (77%) and CRN2-shRNA/GFP-CRN2-S463A cells (80%), respectively (Fig. 6A). Moreover, images at xy, xz, and yz planes showed significant changes in the local F-actin network morphology of these extensions (Figs. 5B and 6B; GFP and GFP-CRN2 cells are not included in 5B). We noted 3 different patterns of F-actin organization in the invadopodia-like extensions (i.e., a diffuse distribution of F-actin, presence of F-actin patches, and an enrichment of F-actin at the rim zone). CRN2-shRNA/GFP cells were characterized by a diffuse distribution of F-actin in the invadopodia-like extensions, which was only marginally present in the other 5 cell lines (Figs. 5B and 6B). A specific feature of the protrusions in

CRN2-shRNA/GFP-CRN2-S463D cells was an enrichment of F-actin at the rim zone (Figs. 5B and 6B), whereas in CRN2-shRNA/GFP-CRN2-S463A cells, F-actin had a more central location (Figs. 5B and 6B). CRN2-shRNA/GFP-CRN2-WT cells were indistinguishable from GFP and GFP-CRN2 cells and showed F-actin patches throughout the volume of the cell protrusions and at the rim zone (Fig. 6B). These results demonstrate that F-actin in invadopodia-like extensions usually occurs in patches that are present throughout the cytoplasm and at the rim zone of the protrusion. After knock-down of CRN2, an aberrant, diffuse distribution of F-actin was found. Furthermore, cells expressing the S463D mutant CRN2 exhibited a distinct enrichment of F-actin at the border of the invadopodia-like extensions.

Expression of S463A and S463D CRN2 Variants Decreases the Turnover of Actin Filaments

FRAP experiments were performed to detect putative changes in CRN2 and actin dynamics at the front of lamellipodia extensions in 2-dimensional cultures of
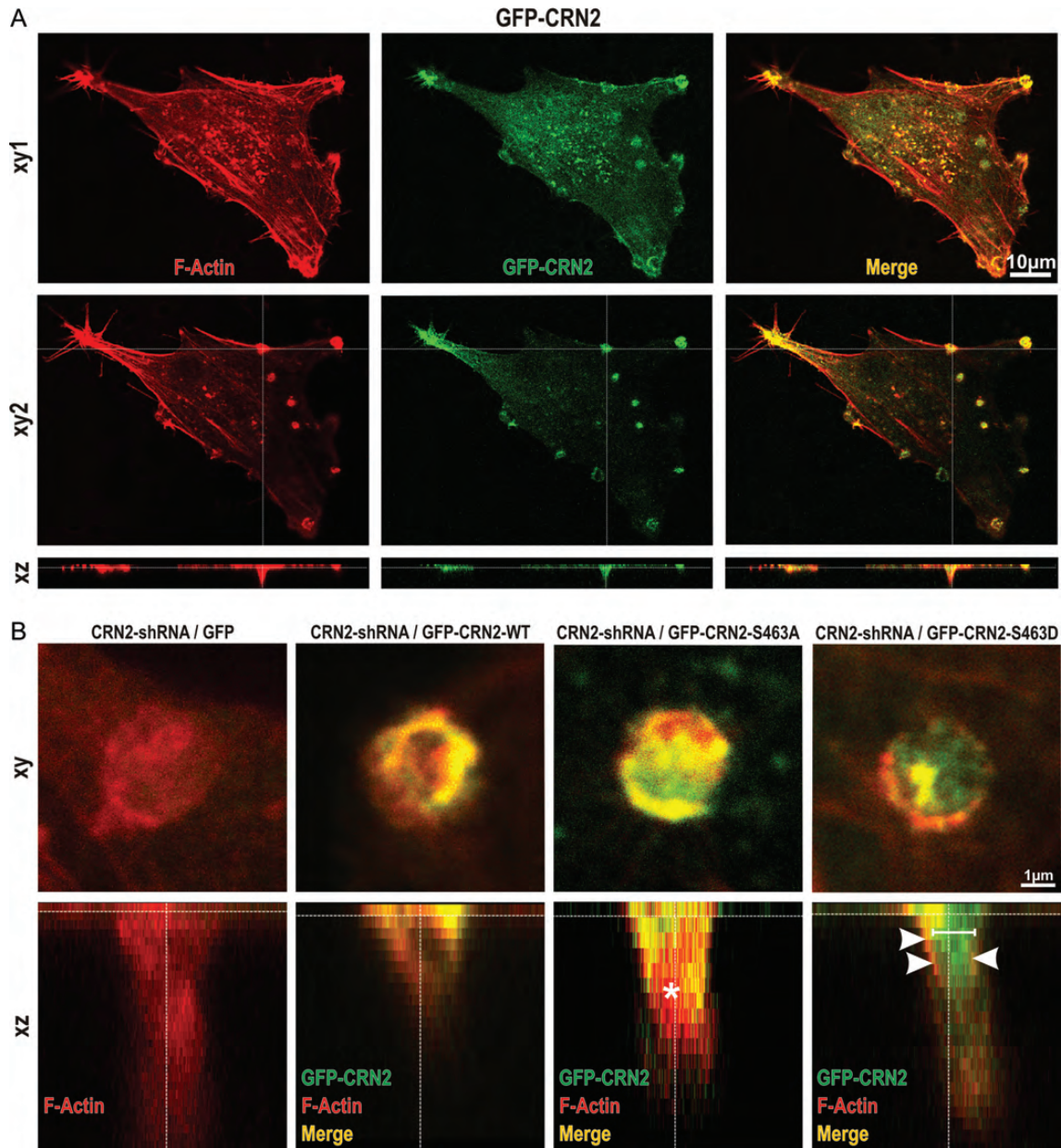
Fig. 5. CRN2 is important for the morphology of the local F-actin network in invadopodia-like cell extensions. Cells were seeded at a low density on 3 μm pore size membrane inserts, and the formation of invadopodia-like protrusions that extended through the pores was monitored by confocal microscopy. (A) As an example, a U373 cell over-expressing GFP-CRN2 is shown. xy1, Z-section above the membrane; xy2, Z-section at the ventral surface of the cell at the level of the membrane pores; xz, example of a xz-plane to visualize invadopodia-like extensions. (B) Images of xy- and xz-planes of individual invadopodia-like extensions at higher magnification characteristic for the indicated cell types. Note, that the diffuse fluorescence signal of GFP in the CRN2 knock-down cell line (CRN2-shRNA/GFP) is hardly detectable in the cell extension. Asterisk denotes centrally enriched F-actin in cells expressing S463A-CRN2. Arrowheads denote F-actin enriched at the rim zone of the extension. Distance label, centrally enriched S463D-CRN2. F-actin was stained by TRITC-phalloidin.

the U373 glioblastoma cell lines. Raw data were first background corrected, followed by a correction of photobleaching of the ROI values with use of the whole cell intensity at each time point, and then normalized to the prebleach intensity. Resulting values were used to calculate the mobile fraction and the half-life time of recovery via bi-exponential curve fitting for both GFP-CRN2 and mCherry-actin. Although clear differences in the mobile fractions (M_f) were detected neither for CRN2 nor for F-actin, the half-life times of fluorescence recovery of both molecules co-elevated by ~0.5 s and 0.8 s in CRN2-shRNA/GFP-CRN2-S463A and CRN2-shRNA/
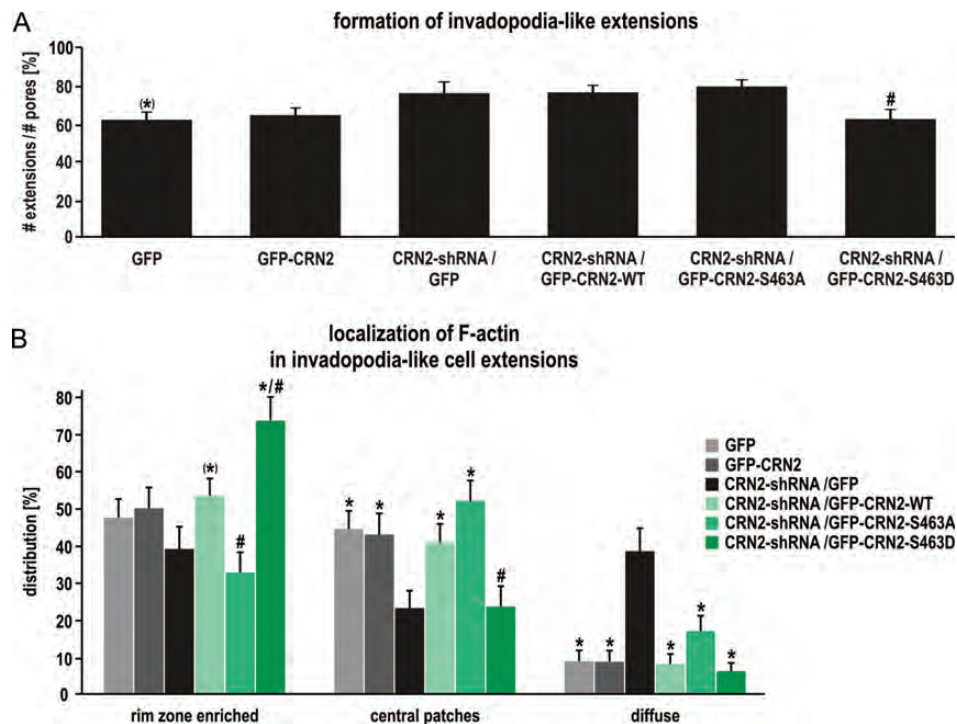
Fig. 6. CRN2 influences the number of cell protrusions and the local distribution of F-actin. (A) Quantitative analysis (mean values and standard errors) of the number of invadopodia-like cell extensions as seen in Fig. 5 normalized to the number of membrane pores per cell. Extensions were counted from 4 to 9 cells from 2 to 3 independent experiments, resulting in a total number of 92–153 extensions that were analyzed per cell line. (B) Subcellular distribution of F-actin in the invadopodia-like extensions. Mean values and standard errors were derived from all invadopodia-like extensions of the cells included in (A). Localizations of F-actin (rim zone, center, or diffuse) are given as relative mean distributions within all extensions of each cell type. *Statistically significant changes, compared with CRN2-shRNA/GFP cells. #Statistically significant changes, compared with CRN2-shRNA/GFP-CRN2-WT cells. See Table 2 for P values.

GFP-CRN2-S463D cells, respectively, compared with CRN2-shRNA/GFP-CRN2-WT cells (Fig. 7).

Discussion

In the present study, we showed that CRN2 is a relevant factor in the regulation of tumor-related cell functions. To compare effects of the level of CRN2 expression, we generated U373 human glioblastoma cell lines with a knock-down of the endogenous CRN2 (CRN2-shRNA/GFP), in which we also expressed GFP-tagged CRN2 (CRN2-shRNA/GFP-CRN2-WT). Furthermore, we used cells with presence of the endogenous CRN2 (GFP) and over-expression of GFP-tagged CRN2 in addition to the endogenous CRN2 (GFP-CRN2). Moreover, we included cells that expressed phospho-resistant S463A (CRN2-shRNA/GFP-CRN2-S463A) and phospho-mimetic S463D mutant CRN2 (CRN2-shRNA/GFP-CRN2-S463D) in the knock-down background, based on the previous finding that phosphorylation at S463 inhibits the cellular activity of CRN2[12] (Table 1, columns 1-3). Expression of GFP-tagged wild-type or mutant CRN2 in U373 cells lacking endogenous CRN2 allows the analysis of phosphorylation-specific effects without interference of the endogenous protein. Moreover, with this design, the specificity of an observed effect in the

knock-down situation can be verified by rescuing the phenotype. Cells expressing only the GFP-tagged CRN2 protein further prove the cellular activity of the GFP-fusion protein.

In Table 1, we have provided a summary of the relative changes caused by knock-down or over-expression of CRN2 for each cellular process analyzed. We have used these relative changes further to calculate a score that displays the overall tumorigenicity of each U373 cell line in vitro and ex vivo. This score indicates that the expression level of CRN2 correlates with the tumorigenicity of the glioblastoma cells. Compared to CRN2-shRNA/GFP cells, GFP cells had a score of 3, CRN2-shRNA/GFP-CRN2-WT cells a score of 10, and GFP-CRN2 cells finally a score of 13. Moreover, CRN2-shRNA/GFP-CRN2-S463A but not CRN2-shRNA/GFP-CRN2-S463D cells also displayed a high score of 12.5. When using CRN2-shRNA/GFP-CRN2-WT cells as reference, a difference in the tumorigenicity of both CRN2 mutants becomes further apparent. Here, CRN2-shRNA/GFP-CRN2-S463A and CRN2-shRNA/GFP-CRN2-S463D cells had scores of 3.5 and -7, respectively.

Indeed, a more detailed view shows that increased expression levels of CRN2 stimulate proliferation, matrix degradation, and invasion rates of U373 glioblastoma cells in vitro. In contrast, increased glioblastoma cell
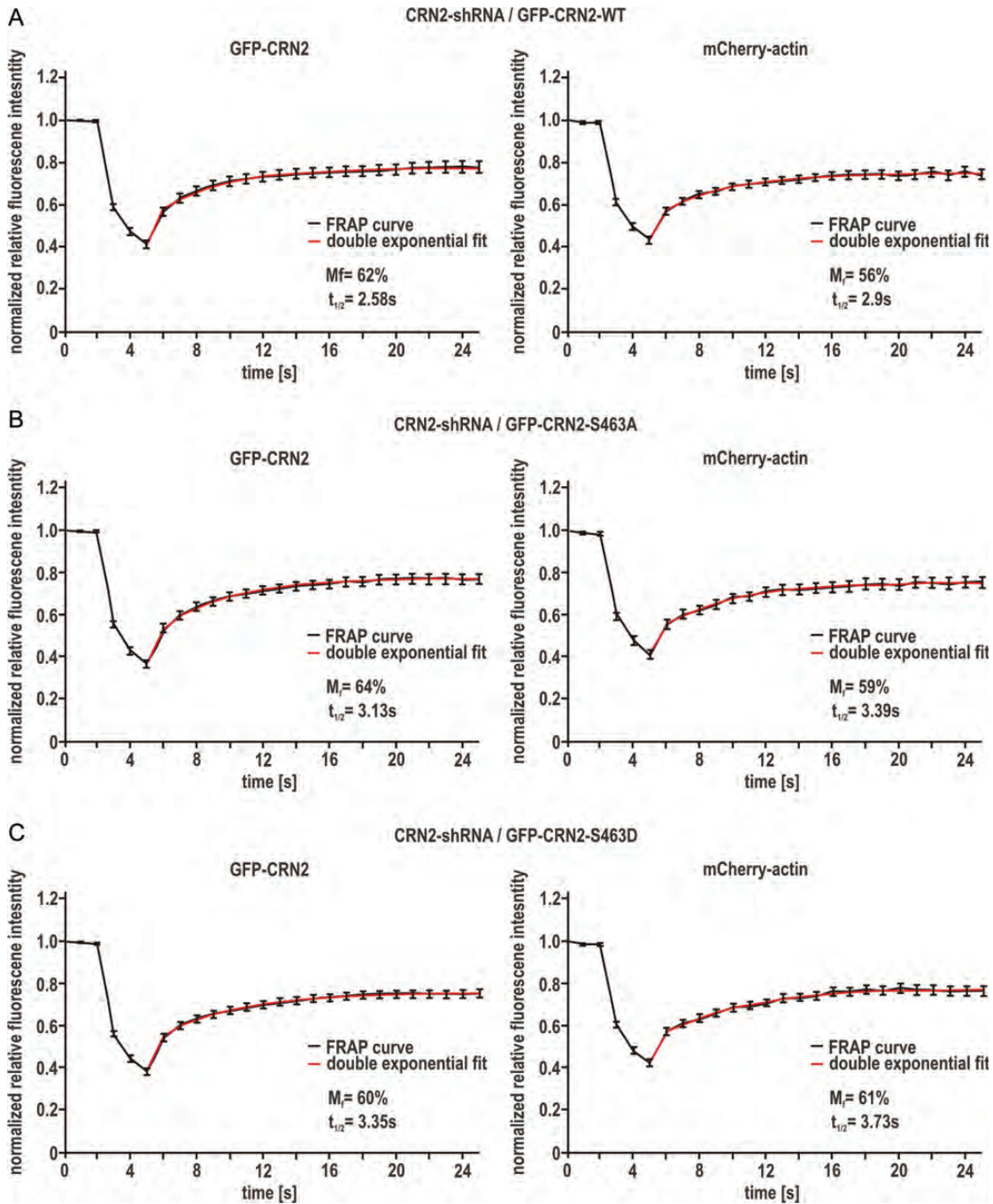
Fig. 7. Half-lives of F-actin structures in the front of lamellipodia are influenced by CRN2. Fluorescence recovery after photobleaching of GFP-CRN2 variants and mCherry-actin were used to calculate mobile fractions (Mf) and half-lives ($t_{1/2}$). Background and photobleaching corrected and normalized mean fluorescence intensities in black (FRAP curves); double-exponential fitting curves in red. Curves and standard errors were calculated from 21 to 28 measurements (a single measurement per cell) from 3 independent experiments.

adhesion and a higher number of invadopodia-like extensions are caused by the knock-down of CRN2. An increased adhesion to collagen I also has been reported in CRN2 knock-down SK-CO15 intestinal epithelial cells.[28] Moreover, our data show that the expression level of CRN2 influences the F-actin organization within invadopodia-like extensions. Changes in the F-actin organization of invadopodia were also observed in cells lacking other F-actin binding proteins (e.g., the F-actin bundling protein

fascin), resulting in shorter invadopodia with a decreased lifetime.[21]

The ex vivo brain slice culture experiments mirror the findings of the in vitro assays. Here, a more invasive tumor phenotype with irregular morphology and increased invasion area and depth is associated with increased CRN2 expression levels. Moreover, expression of the shRNA-resistant GFP-tagged wild-type CRN2 rescues the reduced tumor growth and infiltration

Table 1. Effects of CRN2 expression levels and phospho-mutants on tumor-related cellular processes of U373 glioblastoma cells.

U373 cell line	CRN2 expression endogenous	CRN2 expression GFP-tagged	proliferation	adhesion	matrix degradation	collagen I invasion	number of extensions	F-actin in extensions	irregular tumor morphology	tumor infiltration area	tumor infiltration depth	score	FRAP CRN2 mobile	FRAP CRN2 t₁/₂	FRAP actin mobile	FRAP actin t₁/₂
expression level																
CRN2-shRNA/GFP	no	GFP only	ref value	ref value	ref value	ref value	ref value	diffuse pattern	ref value	ref value	ref value	ref value				
GFP	yes	GFP only	(↑)	↓↓	(↑)	↑	↓	distributed patches	↑	↑	↑↑	3.0				
GFP-CRN2	yes	yes	↑	↓	↑↑	↑↑↑	↓	distributed patches	↑↑↑	↑↑	↑↑↑	13.0				
rescue specific																
CRN2-shRNA/GFP-CRN2-WT	no	yes	↑	=	↑	↑	=	distributed patches	↑↑	↑↑	↑↑	10.0				
CRN2-shRNA/GFP-CRN2-S463A	no	yes	↑	↓↓↓	↑(↑)	↑↑	=	centrally enriched	↑↑↑	↑↑↑↑	↑↑↑	12.5				
CRN2-shRNA/GFP-CRN2-S463D	no	yes	=	↓	↑(↑)	↓	↓	rim zone enriched	↑(↑)	↑↑	↑	3.5				
mutant phosphorylation CRN2																
CRN2-shRNA/GFP-CRN2-WT	no	yes	ref value	ref value	ref value	ref value	ref value	distributed patches	ref value	ref value	ref value	ref value	ref value	ref value	ref value	ref value
CRN2-shRNA/GFP-CRN2-S463A	no	yes	=	↓↓↓	(↑)	↑↑	=	centrally enriched	↑	↑	↑	3.5	=	↑↑	=	↑
CRN2-shRNA/GFP-CRN2-S463D	no	yes	↓	→	=	↓	↓	rim zone enriched	↓	=	↓↓	-7.0	=	↑↑	=	↑↑

Effects of CRN2 knock-down, endogenous CRN2, and over-expressed CRN2 as well as S463A phospho-resistant and S463D phospho-mimetic CRN2 mutants on tumor-related cellular processes of U373 human glioblastoma cells in vitro and ex vivo. Arrows indicate relative changes to the reference value. Score was calculated as sum of (↑) = 0.5, ↑ = 1, ↓ = −1, ↓ = −1. CRN2-shRNA/GFP cells are the reference in the upper part, in the lower part it is CRN2-shRNA/GFP-CRN2-WT.

observed for CRN2 knockdown cells. Another study on CRN2 in gastric cancer showed that the expression level of CRN2 was elevated in gastric cancer and further elevated in lymph node metastases. In addition, knockdown of CRN2 in MKN45 gastric cancer cells inhibited and over-expression of CRN2 in MKN28-NM cells accelerated gap closure in an in vitro wound healing assay. Furthermore, tail vein injection of these CRN2 knockdown cells caused a reduced number of liver metastases in mice.[29] Another coronin found to be involved in cancer is coronin 1A. It has been detected as one of the up-regulated proteins in metastasizing canine mammary carcinomas.[30] Moreover, coronin 1A was found to be elevated in human breast cancer, and over-expression of coronin 1A in SK-BR3 breast cancer cells increased their invasion into Matrigel.[31]

Using CRN2-shRNA/GFP-CRN2-WT cells as reference value, we compared the effects of S463A and S463D mutant CRN2 (Table 1) and found that the state of phosphorylation differentially regulates tumor-related cellular processes. CRN2-shRNA/GFP-CRN2-S463D cells showed less proliferation, collagen I invasion, and invadopodia-like extension formation, whereas no effect was observed for the matrix degradation. In case of the cell adhesion assay cells expressing the S463A mutant, CRN2 had an even more reduced adhesion capacity than the S463D mutant.

In addition, the presence of the 2 CRN2 variants changed the distribution of F-actin patches in invadopodia-like cell extensions. Expression of S463A CRN2 caused an enrichment of F-actin in the center, whereas expression of S463D CRN2 resulted in an accumulation at the rim zone. In the latter case, the colocalization of CRN2 and F-actin is partially lost, and CRN2 instead accumulates in the center of the cell extensions. This observation is consistent with the earlier finding that phosphorylated CRN2 is present in the cytosolic, soluble fraction instead of the membrane fraction containing the submembranous cytoskeleton.[10]

In the brain slice culture experiments, the CRN2-shRNA/GFP-CRN2-S463D cells formed less irregular tumors with decreased infiltration depth. In contrast, a higher fraction of tumors grown from CRN2-shRNA/GFP-CRN2-S463A cells had a more irregular shape and an increased infiltration phenotype. Thus, the expression of the S463D phospho-mimetic CRN2 seems to cause similar effects as the CRN2 knock-down, whereas S463A phospho-resistant CRN2 had effects, comparable with the over-expression of CRN2.

In this respect, we previously found that further stimulation of the constitutively active CK2 markedly increased the level of phosphorylated CRN2, which is less phosphorylated at basal conditions and leads to phosphorylation of serine residue 463. Phosphorylated CRN2 has lost its ability to bundle actin filaments and its inhibitory effect on actin polymerization.[12] The observed stimulatory effects of increased CRN2 levels or phospho-resistant CRN2 on tumor growth and morphology in the present study may be explained by these molecular findings. Both situations would facilitate the formation of a more stable and cross-linked actin

in vitro assays					
proliferation	CRN2-shRNA/GFP	CRN2-shRNA/GFP-CRN2-WT	**matrix degradation**	CRN2-shRNA/GFP	CRN2-shRNA/GFP-CRN2-WT
GFP	3,0E-01		GFP	5,5E-01	
GFP-CRN2	**1,1E-02**		GFP-CRN2	**1,6E-03**	
CRN2-shRNA/GFP-CRN2-WT	**3,0E-02**		CRN2-shRNA/GFP-CRN2-WT	*6,4E-02*	
CRN2-shRNA/GFP-CRN2-S463A	**3,4E-03**	9,1E-01	CRN2-shRNA/GFP-CRN2-S463A	**4,1E-02**	7,2E-01
CRN2-shRNA/GFP-CRN2-S463D	9,3E-01	**4,1E-02**	CRN2-shRNA/GFP-CRN2-S463D	**2,9E-02**	7,8E-01
adhesion	CRN2-shRNA/GFP	CRN2-shRNA/GFP-CRN2-WT	**collagen I invasion**	CRN2-shRNA/GFP	CRN2-shRNA/GFP-CRN2-WT
GFP	**1,0E-12**		GFP	**5,1E-09**	
GFP-CRN2	**8,7E-12**		GFP-CRN2	**4,3E-06**	
CRN2-shRNA/GFP-CRN2-WT	7,5E-01		CRN2-shRNA/GFP-CRN2-WT	1,6E-01	
CRN2-shRNA/GFP-CRN2-S463A	**4,1E-07**	**4,4E-07**	CRN2-shRNA/GFP-CRN2-S463A	**1,3E-03**	**5,0E-03**
CRN2-shRNA/GFP-CRN2-S463D	**5,1E-05**	**8,0E-03**	CRN2-shRNA/GFP-CRN2-S463D	1,9E-01	**6,9E-03**
number of invadopodia	CRN2-shRNA/GFP	CRN2-shRNA/GFP-CRN2-WT	**invadopodia / F-actin central**	CRN2-shRNA/GFP	CRN2-shRNA/GFP-CRN2-WT
GFP	*5,9E-02*		GFP	**4,8E-03**	
GFP-CRN2	1,1E-01		GFP-CRN2	**1,4E-02**	
CRN2-shRNA/GFP-CRN2-WT	9,5E-01		CRN2-shRNA/GFP-CRN2-WT	**1,7E-02**	
CRN2-shRNA/GFP-CRN2-S463A	6,2E-01	5,5E-01	CRN2-shRNA/GFP-CRN2-S463A	**4,6E-04**	1,5E-01
CRN2-shRNA/GFP-CRN2-S463D	8,9E-02	**3,2E-02**	CRN2-shRNA/GFP-CRN2-S463D	9,5E-01	**3,0E-02**
invadopodia / F-actin at rim zone	CRN2-shRNA/GFP	CRN2-shRNA/GFP-CRN2-WT	**invadopodia / F-actin diffuse**	CRN2-shRNA/GFP	CRN2-shRNA/GFP-CRN2-WT
GFP	3,0E-01		GFP	**2,9E-04**	
GFP-CRN2	2,0E-01		GFP-CRN2	**2,7E-04**	
CRN2-shRNA/GFP-CRN2-WT	*7,4E-02*		CRN2-shRNA/GFP-CRN2-WT	**1,9E-04**	
CRN2-shRNA/GFP-CRN2-S463A	4,6E-01	**7,7E-03**	CRN2-shRNA/GFP-CRN2-S463A	**8,9E-03**	9,6E-02
CRN2-shRNA/GFP-CRN2-S463D	**4,0E-04**	**1,6E-02**	CRN2-shRNA/GFP-CRN2-S463D	**8,1E-05**	6,2E-01
ex vivo assays (brain slice cultures)					
tumor infiltration area	CRN2-shRNA/GFP	CRN2-shRNA/GFP-CRN2-WT	**tumor infiltration depth**	CRN2-shRNA/GFP	CRN2-shRNA/GFP-CRN2-WT
GFP	1,7E-01		GFP	1,7E-01	
GFP-CRN2	*7,5E-02*		GFP-CRN2	1,3E-01	
CRN2-shRNA/GFP-CRN2-WT	**1,3E-02**		CRN2-shRNA/GFP-CRN2-WT	4,4E-01	
CRN2-shRNA/GFP-CRN2-S463A	**5,1E-04**	9,5E-01	CRN2-shRNA/GFP-CRN2-S463A	3,7E-01	8,9E-01
CRN2-shRNA/GFP-CRN2-S463D	**2,7E-03**	7,8E-01	CRN2-shRNA/GFP-CRN2-S463D	2,9E-01	6,1E-01

For the indicated experiments P-values were calculated by Student's t test using CRN2-shRNA/GFP as well as CRN2-shRNA/GFP-CRN2-WT cells as reference. Values in bold, $P \leq 0.05$; values in italic just did not reach statistical significance.

network, for example, in cell extensions, and thereby promote tumor cell invasion. Our analyses of the dynamics of CRN2 and actin in the front of lamellipodia revealed elevated half-lives of fluorescence recovery of F-actin in the presence of the CRN2 mutants. An elevated half-life of S463D phospho-mimetic CRN2 (6.56 s vs. 2.27 s of wild-type) previously has been observed by FRAP studies on podosomes.[12] Moreover, 2 large-scale studies of the phospho-proteome of tumor cells further support that nonphosphorylated, rather than phosphorylated, CRN2 is associated with the malignant phenotype. Although phosphorylation of CRN2 at Y301 has been identified in one human non-small cell lung cancer specimen (Supplementary Tables 1 and 2 of Rikova et al[32]) and in the anaplastic large-cell lymphoma cell line SU-DHL-1 (Supplementary Table 8 of Rush et al[33]), CRN2 did not belong to the prominent phospho-proteins.

Our overall data suggest that, beyond an important role in the regulation of the actin cytoskeleton at the molecular level, CRN2 is a relevant factor in tumor biology.

References

1. Smith TF. Diversity of WD-Repeat Proteins. In: Clemen, CS, Eichinger, L, Rybakin, V, eds. The Coronin Family of Proteins. Vol 48: Landes Bioscience, Austin & Springer, New York; 2008. http://www.landesbioscience.com/curie/chapter/3787.

2. Morgan RO, Fernandez MP. Molecular Phylogeny and Evolution of the Coronin Gene Family. In: CS, Clemen, Eichinger, L, Rybakin, V, eds. The Coronin Family of Proteins. Vol 48: Landes Bioscience, Austin & Springer, New York; 2008. http://www.landesbioscience.com/curie/chapter/3820.

3. Eckert C, Hammesfahr B, Kollmar M. A holistic phylogeny of the coronin gene family reveals an ancient origin of the tandem-coronin, defines a new subfamily, and predicts protein function. *BMC Evol Biol.* 2011;11:268.

4. Xavier C-P, Eichinger L, Fernandez MP, Morgan RO, Clemen CS. Evolutionary and Functional Diversity of Coronin Proteins. In: Clemen, CS, Eichinger, L, Rybakin, V, eds. The Coronin Family of Proteins. Vol 48: Landes Bioscience, Austin & Springer, New York; 2008. http://www.landesbioscience.com/curie/chapter/3808.

5. Rybakin V, Clemen CS. Coronin proteins as multifunctional regulators of the cytoskeleton and membrane trafficking. *Bioessays.* 2005;27:625–632.

6. Appleton BA, Wu P, Wiesmann C. The crystal structure of murine coronin-1: a regulator of actin cytoskeletal dynamics in lymphocytes. *Structure.* 2006;14:87–96.

7. McArdle B, Hofmann A. Coronin Structure and Implications. In: Clemen, CS, Eichinger, L, Rybakin, V, eds. The Coronin Family of Proteins. Vol 48: Landes Bioscience, Austin & Springer, New York; 2008. http://www.landesbioscience.com/curie/chapter/3821.

8. Clemen CS, Eichinger L, Rybakin V. The Coronin Family of Proteins. Vol 48: Landes Bioscience, Austin & Springer, New York; 2008. http://www.landesbioscience.com/curie/chapter/3785.

9. Rosentreter A, Hofmann A, Xavier CP, Stumpf M, Noegel AA, Clemen CS. Coronin 3 involvement in F-actin-dependent processes at the cell cortex. *Exp Cell Res.* 2007;313:878–895.

10. Spoerl Z, Stumpf M, Noegel AA, Hasse A. Oligomerization, F-actin interaction, and membrane association of the ubiquitous mammalian coronin 3 are mediated by its carboxyl terminus. *J Biol Chem.* 2002;277:48858–48867.

11. Chan KT, Roadcap DW, Holoweckyj N, Bear JE. Coronin 1C harbours a second actin-binding site that confers co-operative binding to F-actin. *Biochem J.* 2012;444:89–96.

12. Xavier CP, Rastetter RH, Blomacher M, et al. Phosphorylation of CRN2 by CK2 regulates F-actin and Arp2/3 interaction and inhibits cell migration. *Sci Rep.* 2012;2:241.

13. Kimura T, Taniguchi S, Niki I. Actin assembly controlled by GDP-Rab27a is essential for endocytosis of the insulin secretory membrane. *Arch Biochem Biophys.* 2010;496:33–37.

14. Thal D, Xavier CP, Rosentreter A, et al. Expression of coronin-3 (coronin-1C) in diffuse gliomas is related to malignancy. *J Pathol.* 2008;214:415–424.

15. Roadcap DW, Clemen CS, Bear JE. The Role of Mammalian Coronins in Development and Disease. In: Clemen, CS, Eichinger, L, Rybakin, V, eds. The Coronin Family of Proteins. Vol 48: Landes Bioscience, Austin & Springer, New York; 2008. http://www.landesbioscience.com/curie/chapter/3798.

16. Wu L, Peng CW, Hou JX, et al. Coronin-1C is a novel biomarker for hepatocellular carcinoma invasive progression identified by proteomics analysis and clinical validation. *J Exp Clin Cancer Res.* 2010;29:17.

17. Luan SL, Boulanger E, Ye H, et al. Primary effusion lymphoma: genomic profiling revealed amplification of SELPLG and CORO1C encoding for proteins important for cell migration. *J Pathol.* 2010;222:166–179.

18. Ye JH, Zhang J, Xiao C, Kong JQ. Patch-clamp studies in the CNS illustrate a simple new method for obtaining viable neurons in rat brain slices: glycerol replacement of NaCl protects CNS neurons. *J Neurosci Methods.* 2006;158:251–259.

19. Eyupoglu IY, Hahnen E, Heckel A, et al. Malignant glioma-induced neuronal cell death in an organotypic glioma invasion model. *Technical note.* J Neurosurg. 2005;102:738–744.

20. Förster E, Bartosb M, Zhao S. Hippocampal Slice Cultures. In: Poindron, P, Piguet, P, Förster, E, eds. New Methods for Culturing Cells from Nervous Tissues. Vol 1. Basel: Karger; 2005:1–11.

21. Schoumacher M, Goldman RD, Louvard D, Vignjevic DM. Actin, microtubules, and vimentin intermediate filaments cooperate for elongation of invadopodia. *J Cell Biol.* 2010;189:541–556.

22. Koestler SA, Auinger S, Vinzenz M, Rottner K, Small JV. Differentially oriented populations of actin filaments generated in lamellipodia collaborate in pushing and pausing at the cell front. *Nat Cell Biol.* 2008;10:306–313.

23. Clemen CS, Tangavelou K, Strucksberg KH, et al. Strumpellin is a novel valosin-containing protein binding partner linking hereditary spastic paraplegia to protein aggregation diseases. *Brain.* 2010;133: 2920–2941.

24. Noegel AA, Blau-Wasser R, Sultana H, et al. The cyclase-associated protein CAP as regulator of cell polarity and cAMP signaling in Dictyostelium. *Mol Biol Cell.* 2004;15:934–945.

25. Kilmartin JV, Wright B, Milstein C. Rat monoclonal antitubulin antibodies derived by using a new nonsecreting rat cell line. *J Cell Biol.* 1982;93:576–582.

26. Linder S, Wiesner C, Himmel M. Degrading devices: invadosomes in proteolytic cell invasion. *Annu Rev Cell Dev Biol.* 2011;27: 185–211.

27. Murphy DA, Courtneidge SA. The 'ins' and 'outs' of podosomes and invadopodia: characteristics, formation and function. *Nat Rev Mol Cell Biol.* 2011;12:413–426.

28. Samarin SN, Koch S, Ivanov AI, Parkos CA, Nusrat A. Coronin 1C negatively regulates cell-matrix adhesion and motility of intestinal epithelial cells. *Biochem Biophys Res Commun.* 2010;391:394–400.

29. Ren GP, Tian QMD, An YMD, et al. Coronin 3 promotes gastric cancer metastasis via the up-regulation of MMP-9 and cathepsin K. *Mol Cancer.* 2012;11:67.

30. Klopfleisch R, Klose P, Weise C, et al. Proteome of metastatic canine mammary carcinomas: similarities to and differences from human breast cancer. *J Proteome Res.* 2010;9:6380–6391.

31. Kim DH, Bae J, Lee JW, et al. Proteomic analysis of breast cancer tissue reveals upregulation of actin-remodeling proteins and its relevance to cancer invasiveness. *Proteomics Clin Appl.* 2009;3:30–40.

32. Rikova K, Guo A, Zeng Q, et al. Global survey of phosphotyrosine signaling identifies oncogenic kinases in lung cancer. *Cell.* 2007;131:1190–1203.

33. Rush J, Moritz A, Lee KA, et al. Immunoaffinity profiling of tyrosine phosphorylation in cancer cells. *Nat Biotechnol.* 2005;23:94–101.